DOI: 10.31276/VJSTE.2025.0004

Bismuth doping enhances the thermoelectric power of ZnO thin films via structural distortion modulation

Yen Binh Nguyen[1, 2, 3], Trang Thuy Thi Phan[1, 3], Trieu Quang Vo[1, 3], Hoa Thi Lai[3, 4], Thu Bao Nguyen Le[5], Vinh Cao Tran[1, 3], Thang Bach Phan[1, 3, 4], Anh Tuan Thanh Pham[1, 3, 4*]

[1]Laboratory of Advanced Materials, University of Science, Vietnam National University - Ho Chi Minh City, 227 Nguyen Van Cu Street, Cho Quan Ward, Ho Chi Minh City, Vietnam
[2]Faculty of Physics and Engineering Physics, University of Science, Vietnam National University - Ho Chi Minh City, 227 Nguyen Van Cu Street, Cho Quan Ward, Ho Chi Minh City, Vietnam
[3]Vietnam National University - Ho Chi Minh City, Linh Xuan Ward, Ho Chi Minh City, Vietnam
[4]Advanced Materials Technologies Institute, Dong Hoa Ward, Ho Chi Minh City, Vietnam
[5]Faculty of Applied Science, Ho Chi Minh City University of Technology, Vietnam National University - Ho Chi Minh City, 268 Ly Thuong Kiet Street, Dien Hong Ward, Ho Chi Minh City, Vietnam

Received 18 January 2025; revised 18 February 2025; accepted 16 March 2025

Abstract:

The global energy conservation and pollution crisis is compelling the industry to seek methods for harvesting and conserving energy. Microfabrication methods of zinc oxide (ZnO) thin films also play a crucial role in affecting thermoelectric (TE) performance. This study investigates the TE properties of ZnO and Bi-doped ZnO thin films fabricated via radio-frequency (RF) magnetron sputtering. The incorporation of Bi into the ZnO lattice was systematically analysed to determine its impact on residual stress and electrical performance. Structural analysis confirms that Bi doping caused stress relaxation, reducing compressive stress from -1.00 to -0.36 GPa. Complementary insights from micro-Raman spectroscopy revealed Raman shifts, indicating an increase in defect-related modes, specifically an intensified peak at 560 cm^{-1} associated with oxygen vacancy formation. The electrical conductivity of Bi-doped ZnO film reached 776.3 S/cm at 773 K, which was fourfold higher than that of pure ZnO. This enhancement in electrical conductivity played a key role in improving the power factor (PF) of TE materials. The power factor for the Bi-doped ZnO film was enhanced to 463.8 $\mu W/mK^2$ at 773 K compared to pristine ZnO (314.8 $\mu W/mK^2$) under the same conditions.

Keywords: **bismuth doping, structural distortion, thermoelectric power, ZnO thin films.**

Classification numbers: **2.1, 2.2, 2.3**

1. Introduction

The global energy conservation and pollution crisis is compelling the industry to seek methods for harvesting and conserving energy. TE materials can significantly contribute to addressing these issues by converting waste heat into electricity based on the Seebeck effect. The power generation capability of a TE material depends on the PF, defined as $PF=S^2\sigma$, where S is the Seebeck coefficient and σ is the electrical conductivity [1, 2]. High-performance traditional semiconducting TE materials, such as bismuth telluride and lead chalcogenides, are often associated with superior TE properties. However, their toxicity and high cost limit their widespread application [3, 4]. Consequently, the development of non-toxic and environmentally friendly materials has become essential for TE applications.

Microfabrication methods of ZnO thin films also play a crucial role in affecting TE performance. Known techniques such as sol-gel [5], pulsed laser deposition (PLD) [6], and electrochemical deposition [7] have been studied. Additionally, RF magnetron sputtering, with its high deposition rate and good uniformity, can effectively control the structural, morphological, and TE properties of thin-film materials. Some works using RF magnetron sputtering have reported on the TE properties of ZnO-based films [8, 9]. For instance, doping 1% Bi could remarkably reduce the thermal conductivity of ZnO thin films from 6.0 to 3.4 W/mK [9].

ZnO has emerged as a promising alternative due to its unique properties, including abundance, low cost, and high thermal stability [10, 11]. Despite these advantages, ZnO typically exhibits poor electrical properties and high

*Corresponding author: Email: pttanh@hcmus.edu.vn

thermal conductivity, resulting in a low PF value [12, 13]. This limitation hinders its potential for conventional TE applications. Therefore, many strategies have been explored to enhance ZnO's TE performance, such as single and co-doping with foreign atoms or controlling grain boundaries via nanostructuring [14, 15]. For n-type doped ZnO thin films, several studies have focused on group III elements like Al and Ga, resulting in desirable TE properties based on ZnO films [5, 7]. Another study investigated Al-doped ZnO thin films deposited by pulsed laser deposition at temperatures ranging from 300 to 600°C. As a result, the sample deposited at 300°C exhibited the highest PF of 0.55 $\mu W/mK^2$ at 600 K [6]. Meanwhile, several previous reports have mentioned the crucial role of Bi impurity in improving the optical, structural, and photoelectrochemical properties of Bi-doped ZnO films [16, 17]. Only a few studies have investigated Bi-doped ZnO films deposited using magnetron sputtering. In our previous study, the incorporation of Bi into ZnO ceramics led to decreased carrier concentration and lowered electrical conductivity [18]. However, the effect of Bi-doping on the TE properties of ZnO films, specifically deposited by RF magnetron sputtering, has been limitedly studied. Thus, this work focuses on the deposition of undoped ZnO and 1% Bi-doped ZnO thin films using the RF sputtering method. The TE and structural properties of these films are presented and discussed.

2. Materials and methods

Pure ZnO and 1% at Bi-doped ZnO thin films were deposited on glass substrates with a film thickness of ~600 nm using RF magnetron sputtering (Leybold Univex-450). The two-inch sputtering targets were homemade from commercial powders, including ZnO (99.9%, Merck) and Bi_2O_3 (99.995%, Alfa Aesar). For the Bi-doped ZnO target, the powders were mixed at an atomic ratio of Bi:Zn = 1:99, corresponding to 1% Bi doping. The powder mixture was then wet ball-milled with distilled water for five hours using alumina grinding media. Subsequently, the mixture was dried at 120°C for 24 hours to remove residual moisture, followed by a cold-pressing and sintering process at 1400°C in air for three hours. Finally, the sintered targets were polished and cleaned to prepare for the sputtering process. The substrate-target distance was fixed at 5 cm. The base and working pressures were set at 4×10^{-6} Torr and 3.5 mTorr, respectively. The sputtering power was maintained at 120 W, and the substrate temperature was controlled at 200°C during the deposition process.

The crystalline structure of the films was analysed by X-ray diffraction (XRD) measurements (Bruker D8-Advance). A Linseis LSR-3 apparatus was employed to measure the temperature-dependent Seebeck coefficient and electrical conductivity of the films. Raman scattering microscopy (Horiba XploRa Plus) with a 532-nm excitation source and a resolution of 3 cm^{-1} was utilised to examine chemical bonds in the samples.

3. Results and discussion

The XRD patterns of the pure ZnO and 1% Bi-doped ZnO thin films with the 2θ scanning angle of 25-40° are shown in Fig. 1. The films are identified as polycrystalline with a hexagonal structure of ZnO [19]. From the results, the pure ZnO film exhibits crystal planes (100), (002), and (101) located at approximately 31.6, 34.3, and 36.1° respectively, which are well-matched with the Joint Committee on Powder Diffraction Standards (JCPDS) 036-1451 database [20].

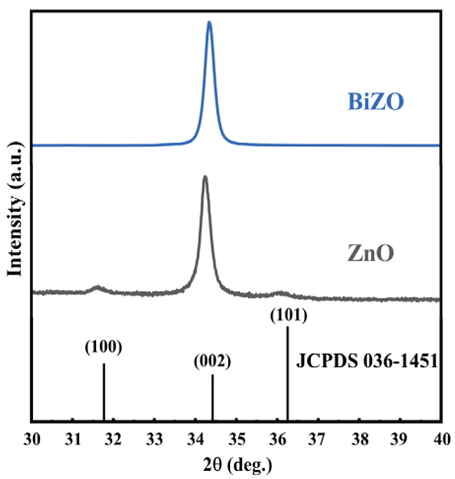

Fig. 1. X-ray diffraction patterns of pure ZnO and 1% at Bi-doped ZnO thin films. Source: Authors' calculation.

No secondary phases were observed in either film, indicating that Bi impurities are effectively incorporated into the ZnO lattice. Both samples show a strong intensity of the diffraction peak (002); with the addition of Bi content, there is an increase in intensity and the disappearance of the (100) and (101) peaks in the Bi-doped sample. This suggests that the doping process enhances crystallinity and promotes a stronger preferred orientation along the c-axis, which is perpendicular to the substrate.

The crystallite size of both films was calculated using Scherrer's formula [21]:

$$D = \frac{0.9\lambda}{\beta\cos\theta}$$

where D is the average crystalline size of the crystal, λ is the X-ray wavelength that the source used (0.154 nm), β is the full width at half maximum, and θ is the Bragg angle of the (002) peak.

Additionally, to clearly understand the change in structural properties, the lattice constant c of the samples was evaluated using the formula for hexagonal structures [22]:

$$c = 2d_{(002)} = \frac{\lambda}{\sin\theta}$$

In addition, doping could cause impacts on the residual stress (ε) inside thin films, ε values of films can be determined using the biaxial stress model [23]:

$$\varepsilon = \frac{2C_{13}^2 - C_{33}(C_{11} + C_{12})}{2C_{13}} \times \frac{c - c_o}{c_o}$$

where c is the lattice parameter of the strained films estimated from the XRD data above; c_o is the unstrained lattice parameter of ZnO powder (0.52066 nm); C_{ij} are the bulk ZnO elastic stiffness constants (C_{11}=208.8 GPa, C_{12}=119.7 GPa, C_{13}=104.2 GPa, and C_{33}=213.8 GPa).

Table 1. Crystallite size, lattice parameter c, and residual stress ε along the (002) plane between pure and Bi-doped samples.

Samples	Crystallite size (nm)	c (nm)	ε (GPa)
ZnO	25.49	0.523	-1.00
1% Bi-doped ZnO	27.72	0.521	-0.36

The calculated values for crystallite size, lattice constant c, and residual stress of ZnO and Bi-doped ZnO films are shown in Table 1. Upon doping with Bi, the crystallite size increases from 25.49 to 27.72 nm, indicating the incorporation of Bi into the ZnO lattice. Moreover, the lattice parameter c of both films is higher than that of ZnO powder (0.52066 nm) [24], which could suggest the development of compressive stress in the films. It should be noted that doping with impurities with a larger ionic radius than the host ion usually leads to lattice compressive stress. However, in this case, the ionic radius of Bi^{3+} (0.103 nm) is larger than that of Zn^{2+} (0.074 nm), giving the opposite trend. Therefore, the finding in our study could be due to the mismatch between the radii of foreign and host atoms [25]. A similar effect has been observed in studies of ZnO doped with elements having larger ionic radii, where the substitution of dopant into host ions results in more oxygen vacancies in the lattice [26, 27].

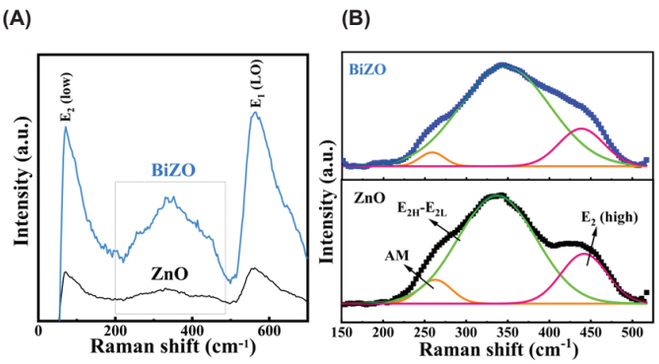

Fig. 2. Raman spectra of pure ZnO and Bi-doped ZnO thin films: (A) survey spectra, **(B)** deconvolution spectra in the wavelength number of 150-500 cm^{-1}. Source: Authors' calculation.

For wurtzite ZnO, group theoretical analysis reveals the nature of the optical phonon modes at the Γ point, which arise from the crystal's symmetry. These modes can be classified as below [28]:

$$\Gamma = A_1 + 2B_1 + E_1 + 2E_2$$

where the A_1 and E_1 modes are polar and split into transverse optical (TO) and longitudinal optical (LO) phonons, both of which are Raman and infrared active. The E_2 modes are non-polar and active, comprising two components: E_2 (high) and E_2 (low). The B_1 mode is Raman inactive (silent modes) [29]. The room temperature micro-Raman spectra of pure ZnO and Bi-doped ZnO films recorded in the spectral region from 50 to 700 cm^{-1} are presented in Fig. 2A. It is observed that both ZnO and Bi-doped ZnO films exhibit two distinct peaks at 90 and 560 cm^{-1}. The sharp and intense peak at around 90 cm^{-1} is assigned to the E_2 (low) mode, which represents vibrations of the zinc atom in the lattice [30]. The Raman band at 560 cm^{-1} can be attributed to the formation of defects such as zinc interstitials and oxygen vacancies. In comparison with the pristine sample, the band shows a slightly higher intensity when doped, indicating a higher concentration of defects [31]. This result is consistent with the XRD results showing the reduction of compressive stress in Bi-doped ZnO films. Additionally, both films exhibited a broad spectral peak, which may be the overlap of multiple peaks oscillating in the range of 150 to 500 cm^{-1}. The spectral deconvolution of the ZnO and Bi-doped ZnO films was performed as shown in Fig. 2B. The peak at 448 cm^{-1} corresponds to a non-polar optical phonon E_2 (high), which depicts the vibration of oxygen atoms in the lattice

and is the characteristic peak of wurtzite ZnO, while the peak at 345 cm^{-1} is assigned to the E_{2H}-E_{2L} multi-phonon process [32, 33]. The broad peak related to 265 cm^{-1} can be assigned to anomalous modes (AM), where the AM has been stated as originating from host-lattice defects that naturally arise concerning the doping [29, 34].

Combining the Raman and XRD results, the formation of oxygen vacancies in the Bi-doped ZnO film is predicted. This observation can be explained by the incorporation of Bi into the ZnO lattice, which induces structural distortion due to the substitution of Zn^{2+} by larger Bi^{3+} ions. Hence, to stabilise the lattice structure, the formation of vacancy-related defects can be dominant. Additionally, because Bi^{3+} has a higher charge than Zn^{2+}, a charge imbalance arises. Thus, the formation of oxygen vacancies releases free electrons, leading to charge compensation for maintaining charge neutrality [35]. Another reason can originate from the difference in coordination sites of Bi^{3+} and Zn^{2+}. Specifically, Zn^{2+} is mainly located at tetrahedral [ZnO_4] sites, whereas Bi^{3+} is situated at octahedral [BiO_6] sites. Therefore, the substitution of Zn^{2+} by Bi^{3+} leads to a transfer from [BiO_6] sites to [BiO_4] sites, thus increasing oxygen vacancies in the Bi-doped ZnO film. This effect is similar to the substitution of Zn^{2+} by Ga^{3+} in the ZnO lattice, as demonstrated in our previous study [36]. However, the substitution of Zn^{2+} by Bi^{3+} will be investigated in the next study.

The temperature dependence of electrical conductivity (σ) for both pristine and 1% Bi-doped ZnO films is shown in Fig. 3A. It can be observed that both samples exhibit increased electrical conductivity across the entire measured temperature range, from room temperature (RT) to 773 K, indicating clear semiconducting behaviour. At the highest measured temperature (773 K), the conductivity of the pristine ZnO film reaches approximately 179.2 S/cm, whereas the Bi-doped ZnO film shows a fourfold increase in σ to 776.3 S/cm. The superior conductivity of Bi-doped ZnO compared to ZnO is attributed to additional charge carriers introduced through Bi substitution in the ZnO structure [37]. The Seebeck coefficient (S) of the samples as a function of temperature is shown in Fig. 3B. The negative values along the S-axis indicate the n-type conduction behaviour of the material. Throughout the entire temperature range, the absolute value of S for the pristine ZnO film is significantly higher than that of the Bi-doped sample, primarily due to the lower carrier concentration in the undoped ZnO [38]. At 773 K, the absolute Seebeck coefficient reaches approximately 132.5 μV/K for pristine ZnO and 77.3 μV/K for the Bi-doped ZnO film. The temperature dependence of the PF for the thin films is shown in Fig. 3C. Despite

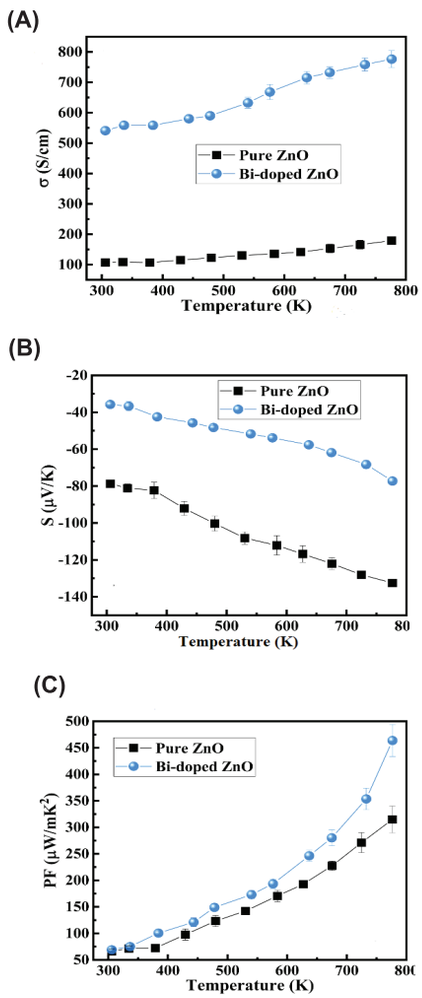

Fig. 3. Temperature-dependent (A) electrical conductivity; (B) Seebeck coefficient; and (C) power factor of pure ZnO and Bi-doped ZnO thin films.

the typical trade-off between electrical conductivity and the Seebeck coefficient, the PF values of the Bi-doped ZnO sample remain consistently higher than those of the undoped ZnO over the entire temperature range. The pure ZnO film exhibits a PF value of 314.8 μW/mK², while the Bi-doped ZnO film achieves a significantly higher maximum PF of 463.8 μW/mK² at 773 K. This improvement is attributed to the significantly higher electrical conductivity in the Bi-doped ZnO, which plays a key role in enhancing the PF, leading to a monotonic increase in PF values as the temperature rises. This result highlights the effectiveness of Bi doping in improving the TE performance of ZnO thin films. Notably, this PF value surpasses those reported for Al-doped ZnO nanopowder synthesised by RF plasma (PF~400 μW/mK² at 1073 K) and for a 5% Ga-doped ZnO thin film (PF~440 μW/mK² at 573 K) [39, 40].

4. Conclusions

In this study, Bi-doped ZnO thin films were successfully deposited using RF sputtering, and their structural and TE properties were systematically investigated. XRD analysis confirmed the stress relaxation with a reduction in compressive stress. Raman spectroscopy revealed an increase in defect-related vibrational modes, indicating the formation of oxygen vacancies due to Bi incorporation. The oxygen vacancies contributed to an increased carrier concentration, which significantly influenced the electrical and TE performance of the films. Although the Seebeck coefficient of the Bi-doped ZnO film remained low, the electrical conductivity of the doped film was fourfold higher than that of pure ZnO, leading to a substantial improvement in PF. The maximum power factor of the Bi-doped ZnO film was 463.8 μW/mK² at 773 K, compared to 314.8 μW/mK² for pristine ZnO under the same conditions. These results demonstrate that Bi doping effectively enhances the TE performance of ZnO thin films, with electrical conductivity playing a dominant role in power factor enhancement.

CRediT author statement

Yen Binh Nguyen: Investigation, Writing original draft; Trang Thuy Thi Phan, Trieu Quang Vo, Hoa Thi Lai, Thu Bao Nguyen Le: Data curation; Vinh Cao Tran: Resources, Methodology; Thang Bach Phan: Methodology, Funding acquisition; Anh Tuan Thanh Pham: Conceptualisation, Data curation, Reviewing and Editing.

ACKNOWLEDGEMENTS

This research is funded by the National Foundation for Science and Technology Development of Vietnam (NAFOSTED) under the grant number 103.02-2021.54.

COMPETING INTERESTS

The authors declare that there is no conflict of interest regarding the publication of this article.

REFERENCES

[1] Y. Jiang, B. Su, J. Yu, et al. (2024), "Exceptional figure of merit achieved in boron-dispersed GeTe-based TE composites", *Nature Communications*, **15**, DOI: 10.1038/s41467-024-50175-6.

[2] H.J. Wu, L.D. Zhao, F.S. Zheng, et al. (2014), "Broad temperature plateau for TE figure of merit ZT>2 in phase-separated $PbTe_{0.7}S_{0.3}$", *Nature Communications*, **5**, DOI: 10.1038/ncomms5515.

[3] H. Mamur, M.R.A. Bhuiyan, F. Korkmaz, et al. (2018), "A review on bismuth telluride (Bi_2Te_3) nanostructure for TE applications", *Renewable and Sustainable Energy Reviews*, **82**, pp.4159-4169, DOI: 10.1016/j.rser.2017.10.112.

[4] L. Zhao, Y. He, H. Zhang, et al. (2018), "Enhancing the TE property of Bi_2Te_3 through a facile design of interfacial phonon scattering", *Journal of Alloys and Compounds*, **768**, pp.659-666, DOI: 10.1016/j.jallcom.2018.07.324.

[5] A. Tomeda, T. Ishibe, T. Taniguchi, et al. (2018), "Enhanced TE performance of Ga-doped ZnO film by controlling crystal quality for transparent TE films", *Thin Solid Films*, **666**, pp.185-190, DOI: 10.1016/j.tsf.2018.09.045.

[6] S. Saini, P. Mele, H. Honda, et al. (2014), "TE properties of Al-doped ZnO thin films", *Journal of Electronic Materials*, **43(6)**, pp.2145-2150, DOI: 10.1007/s11664-014-2992-x.

[7] M.M.R.A. Fartoos, A. Roy, T.K. Mallick, et al. (2024), "A semi-transparent TE glazing nanogenerator with aluminium doped zinc oxide and copper iodide thin films", *Communications Engineering*, **3**, DOI: 10.1038/s44172-024-00291-4.

[8] N.V. Schäuble, Y.E. Romanyuk, S. Yoon, et al. (2012), "TE properties of nanostructured Al-substituted ZnO thin films", *Thin Solid Films*, **520(23)**, pp.6869-6875, DOI: 10.1016/j.tsf.2012.07.046.

[9] F.C. Correia, J.M. Ribeiro, A. Ferreira, et al. (2023), "The effect of Bi doping on the thermal conductivity of ZnO and ZnO:Al thin films", *Vacuum*, **207**, DOI: 10.1016/j.vacuum.2022.111572.

[10] M. Saeed, H.M. Marwani, U. Shahzad, et al. (2024), "Recent advances, challenges, and future perspectives of ZnO nanostructure materials towards energy applications", *Chemical Record*, **24**, DOI: 10.1002/tcr.202300106.

[11] M. Carofiglio, S. Barui, V. Cauda, et al. (2020), "Doped zinc oxide nanoparticles: Synthesis, characterization and potential use in nanomedicine", *Applied Sciences (Switzerland)*, **10(15)**, DOI: 10.3390/app10155194.

[12] B. Duan, Y. Li, J. Li, et al. (2020), "Regulation of oxygen vacancy and reduction of lattice thermal conductivity in ZnO ceramic by high temperature and high pressure method", *Ceramics International*, **46(16)**, pp.26176-26181, DOI: 10.1016/j.ceramint.2020.07.115.

[13] Z.X. Huang, Z.A. Tang, J. Yu, et al. (2011), "Thermal conductivity of nanoscale polycrystalline ZnO thin films", *Physica B: Condensed Matter*, **406(4)**, pp.818-823, DOI: 10.1016/j.physb.2010.11.099.

[14] S. Sulaiman, I. Sudin, U.M.B.A. Naib, et al. (2022), "Review of the nanostructuring and doping strategies for high-performance ZnO TE materials", *Crystals*, **12(8)**, DOI: 10.3390/cryst12081076.

[15] C. Gayner, K.K. Kar (2016), "Recent advances in TE materials", *Progress in Materials Science*, **83**, pp.330-382, DOI: 10.1016/j.pmatsci.2016.07.002.

[16] M. Vadivel, S. Gopalakrishnan, R.R. Babu, et al. (2022), "Influence of Bi doping concentrations on the structural, morphological, dielectric, optical and magnetic properties of ZnO nanoparticles", *Journal of Superconductivity and Novel Magnetism*, **35(12)**, pp.3647-3659, DOI: 10.1007/s10948-022-06418-y.

[17] H.R. Khan, R. Akram, M. Aamir, et al. (2023), "Investigations of photoelectrochemical performance of polycrystalline Bi-doped ZnO thin films", *Journal of Physics and Chemistry of Solids*, **181**, DOI: 10.1016/j.jpcs.2023.111529.

[18] T.M. Bui, D.C. Truong, P.Y. Nguyen, et al. (2022), "Structural, electrical and TE characterizations of bismuth-doped ZnO ceramic material", *Science and Technology Development Journal*, **25(3)**, pp.2489-2496, DOI: 10.32508/stdj.v25i3.3935.

[19] E.Ş. Tüzemen, S. Eker, H. Kavak, et al. (2009), "Dependence of film thickness on the structural and optical properties of ZnO thin films", *Applied Surface Science*, **255(12)**, pp.6195-6200, DOI: 10.1016/j.apsusc.2009.01.078.

[20] J. Gaur, S. Kumar, M. Zineddine, et al. (2024), "CTAB-crafted ZnO nanostructures for environmental remediation and pathogen control", *Scientific Reports*, **14(1)**, DOI: 10.1038/s41598-024-65783-x.

[21] P. Perumal, N.A. Sathakkathulla, K. Kumaran, et al. (2024), "Green synthesis of zinc oxide nanoparticles using aqueous extract of shilajit and their anticancer activity against HeLa cells", *Scientific Reports*, **14(1)**, DOI: 10.1038/s41598-024-52217-x.

[22] G.M. Abdelghani, A.B. Ahmed, A.B.A. Zubaidi (2022), "Synthesis, characterization, and the influence of energy of irradiation on optical properties of ZnO nanostructures", *Scientific Reports*, **12(1)**, DOI: 10.1038/s41598-022-24648-x.

[23] P.W. Chi, C.W. Su, D.H. Wei (2017), "Internal stress induced natural self-chemisorption of ZnO nanostructured films", *Scientific Reports*, **7**, DOI: 10.1038/srep43281.

[24] H. Ennaceri, M. Boujnah, D. Erfurt, et al. (2019), "Influence of stress on the photocatalytic properties of sprayed ZnO thin films", *Solar Energy Materials and Solar Cells*, **201**, DOI: 10.1016/j.solmat.2019.110058.

[25] S. Lavanya, T.R. Kumar, B. Prakash, et al. (2024), "Effect of Bi doping on the opto-electronic properties of ZnO nanoparticles for photodetector applications", *Journal of Photochemistry and Photobiology A: Chemistry*, **446**, DOI: 10.1016/j.jphotochem.2023.115119.

[26] A.A. Dakhel, M.E. Hilo (2010), "Ferromagnetic nanocrystalline Gd-doped ZnO powder synthesized by coprecipitation", *Journal of Applied Physics*, **107(12)**, DOI: 10.1063/1.3448026.

[27] D. Arora, K. Asokan, A. Mahajan, et al. (2016), "Structural, optical and magnetic properties of Sm doped ZnO at dilute concentrations", *RSC Advances*, **6(81)**, pp.78122-78131, DOI: 10.1039/c6ra12905f.

[28] C. Jayachandraiah, G. Krishnaiah (2015), "Erbium induced Raman studies and dielectric properties of Er-doped ZnO nanoparticles", *Advanced Materials Letters*, **6(8)**, pp.743-748, DOI: 10.5185/amlett.2015.5801.

[29] R.S. Zeferino, M.B. Flores, U. Pal (2011), "Photoluminescence and Raman scattering in Ag-doped ZnO nanoparticles", *Journal of Applied Physics*, **109(1)**, DOI: 10.1063/1.3530631.

[30] A. Momot, M.N. Amini, G. Reekmans, et al. (2017), "A novel explanation for the increased conductivity in annealed Al-doped ZnO: An insight into migration of aluminum and displacement of zinc", *Physical Chemistry Chemical Physics*, **19(40)**, pp.27866-27877, DOI: 10.1039/c7cp02936e.

[31] R. Cuscó, E.A. Lladó, J. Ibáñez, et al. (2007), "Temperature dependence of Raman scattering in ZnO", *Physical Review B*, **75(16)**, DOI: 10.1103/PhysRevB.75.165202.

[32] R.F. Zhuo, H.T. Feng, Q. Liang, et al. (2008), "Morphology-controlled synthesis, growth mechanism, optical and microwave absorption properties of ZnO nanocombs", *Journal of Physics D: Applied Physics*, **41(18)**, DOI: 10.1088/0022-3727/41/18/185405.

[33] A. Sharma, B.P. Singh, S. Dhar, et al. (2012), "Effect of surface groups on the luminescence property of ZnO nanoparticles synthesized by sol-gel route", *Surface Science*, **606(3-4)**, pp.L13-L17, DOI: 10.1016/j.susc.2011.09.006.

[34] O. Dobrozhan, A. Opanasyuk, M. Kolesnyk, et al. (2015), "Substructural investigations, Raman, and FTIR spectroscopies of nanocrystalline ZnO films deposited by pulsed spray pyrolysis", *Physica Status Solidi (A) Applications and Materials Science*, **212(12)**, pp.2915-2921, DOI: 10.1002/pssa.201532324.

[35] A.M.H. Flores, E.L. Hipólito, L.M.T. Martínez, et al. (2019), "Photocatalytic H_2 production and CO_2 reduction on Cu, Ni-doped ZnO: Effect of metal doping and oxygen vacancies", *Journal of Materials Science: Materials in Electronics*, **30(20)**, pp.18506-18518, DOI: 10.1007/s10854-019-02204-0.

[36] A.T.T. Pham, T.A. Luu, N.K. Pham, et al. (2020), "Multi-scale defects in ZnO TE ceramic materials co-doped with In and Ga", *Ceramics International*, **46(8)**, pp.10748-10758, DOI: 10.1016/j.ceramint.2020.01.084.

[37] F. Chouikh, Y. Beggah, N. Ariche, et al. (2019), "A comparative study of Al and Bi addition in the transparent conductive ZnO thin films prepared by spray ultrasonic method", *International Journal of Thin Film Science and Technology*, **8(3)**, pp.101-112, DOI: 10.18576/ijtfst/080302.

[38] M.M.R.A. Fartoos, A. Roy, T.K. Mallick, et al. (2023), "Advancing TE materials: A comprehensive review exploring the significance of one-dimensional nano structuring", *Nanomaterials*, **13(13)**, DOI: 10.3390/nano13132011.

[39] H. Cheng, X.J. Xu, H.H. Hung, et al. (2009), "Characterisation of Al-doped ZnO TE materials prepared by RF plasma powder processing and hot press sintering", *Ceramics International*, **35(8)**, pp.3067-3072, DOI: 10.1016/j.ceramint.2009.04.010.

[40] A.T.T. Pham, H.K.T. Ta, Y.R. Liu, et al. (2018), "Effect of annealing temperature on TE properties of Ga and In dually doped - ZnO thin films", *Journal of Alloys and Compounds*, **747**, pp.156-165, DOI: 10.1016/j.jallcom.2018.02.349.